TIME OF ARRIVAL DELINEATION IN ECHO TRACES
FOR REFLECTION ULTRASOUND TOMOGRAPHY

Bhaskara R Chintada[1],   *Richard Rau*[1],   *Orcun Goksel*[1,2]

[1] Computer-assisted Applications in Medicine, ETH Zurich, Switzerland
[2] Department of Information Technology, Uppsala University, Sweden

ABSTRACT

Ultrasound Computed Tomography (USCT) is an imaging method to map acoustic properties in soft tissues, e.g., for the diagnosis of breast cancer. A group of USCT methods rely on a passive reflector behind the imaged tissue, and they function by delineating such reflector in echo traces, e.g., to infer time-of-flight measurements for reconstructing local speed-of-sound maps. In this work, we study various echo features and delineation methods to robustly identify reflector profiles in echos. We compared and evaluated the methods on a *multi-static* data set of a realistic breast phantom. Based on our results, a RANSAC based outlier removal followed by an active contours based delineation using a new "edge" feature we propose that detects the first arrival times of echo performs robustly even in complex media; in particular 2.1 times superior to alternative approaches at locations where diffraction effects are prominent.

Index Terms— Speed of sound, Reflector delineation, Active contours

1. INTRODUCTION

Ultrasound Computed Tomography (USCT) images the local ultrasound wave propagation parameters such as speed-of-sound (SoS), attenuation, and refractive indices [1], since these parameters may facilitate differentiation of different tissue compositions and thereby potentially helping in diagnosis. For example, USCT may help in breast cancer diagnosis [1, 2]. One USCT approach using conventional ultrasound probes functions by placing an acoustic reflector on the opposite side of imaged tissue [3–6]. In this approach, the transducer elements are operated in *multi-static* mode, i.e., after the transmission (Tx) of a wave by a single element of the transducer array, all adjacent transducer elements simultaneously receive (Rx) the radio-frequency (RF) echo signals. This procedure is repeated for each transducer element. Based on such multi-static acquisition, the time-of-flight (ToF) for all Tx-Rx combinations are computed to be used in a subsequent CT image reconstruction process, such as for local SoS maps [5] or, using the amplitudes at those instances, for attenuation maps [6]. The key to all such reconstruction outcome is a precise ToF estimation that is input to any CT algorithm.

Several ToF estimation methods have been explored in literature: Simple approaches utilize the maximum echo amplitude or max of amplitude gradient [7] (to find the rising edge), or similarly the first peak of these after an approximate time point. In [8] ToF values are estimated by the center-of-mass of a match filtered RF A-line by an assumed reflector echo pattern. Similarly, cross-correlation of each Rx A-line with a reference signal obtained, e.g., via measurements in water can also be utilized. Since processing each Rx A-line is very likely to produce outliers, an important prior in ToF estimation

across several Rx lines is their expected pseudo connectivity in Rx-time space; i.e., the reflector echo in two consecutive Rx channels are expected temporally nearby. Exploiting this, in [9] weighted combination of echo amplitude and gradient values is used in an active contours framework [10]. Dynamic programming based reflector delineation was introduced in [5] using the positive or negative peaks of reflector echoes around an expected arrival time frame.

Although functioning well fairly homogeneous media, the above methods have difficulty in complex heterogeneous media due to several other reflections from tissue layers and wavefront distortions such as refraction, diffraction, and aberration. In such scenarios what signal features to use is also not clear. The features based on echo shape (e.g., point of symmetry, maximum peak/minimum peak, center-of-mass, match filtering, and reference correlation) are highly influenced by dispersion and diffraction effects; so methods that work in simple settings often do not translate successfully to complex media. A systematic study of different signal features and their use in robust outlier removal methods for smooth delineation of ToF across Rx echo traces is missing in the literature. We present this herein based on manually delineated signals in a complex, realistic breast ultrasound phantom, by comparing several features from the literature and that we propose herein.

2. METHODS

2.1. Dataset

128 multi-static ultrasound images were acquired on breast ultrasound phantom (Model 0459, CIRS Inc.USA) using a 128 element ultrasound transducer (L14/5-38) operated at 5 MHz center frequency by a research ultrasound machine (SonixTouch, Ultrasonix, Richmond, Canada). Given 40 MHz sampling, each such pre-beamformed ultrasound RF frame is then (#RF-time-points x #Rx-channels) 4152 x 128 in size. Reflector location (i.e. ToF) in each A-line was annotated on ultrasound images for evaluation.

2.2. Ultrasound Reflection Tomography

A typical reflection-mode USCT setup is shown in Fig. 1a, with a passive reflector on the opposite side of an imaged tissue sample. A sample (non-refracting) shortest acoustic path of a wavefront emitted from a Tx element, reflected from the reflector, and arriving at an Rx element is illustrated by Fig. 1a ①. Then, the following forward problem [5] of tomographic reconstruction $\mathbf{Ls} = \mathbf{t}$ relates a column vector $\mathbf{t}$ of integral ToF values between all Tx-Rx element combinations to the tissue *slowness* (1/SoS) values $\mathbf{s}$, through a system matrix $\mathbf{L}$ encoding the ray integrals for each wavefront discretized onto a 2D pixel grid of local slowness values. Note that $\mathbf{L}$ is constant for given transducer geometry and reflector position. Given
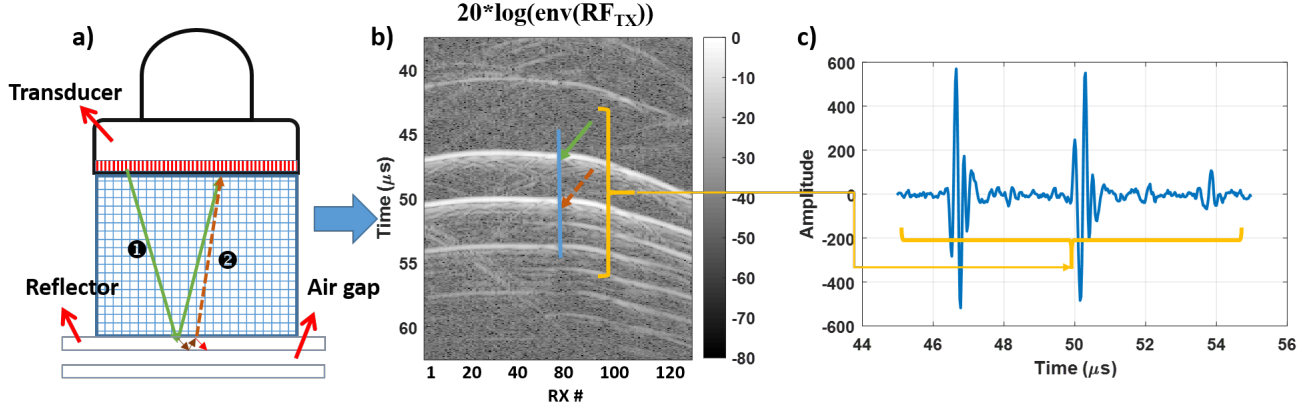
Fig. 1. (a) Schematic of the experimental setup for data acquisition. An incident acoustic wave reflects from the phantom-plexiglas inter-face ① while some of it transmits through plexiglas reflecting back entirely (with opposite phase) from the onset of air gap, part of it reaching the transducer ②. Part of the wave oscillating with the plexiglas causes multiple reflections, complicating a delineation. (b) A prebeam-formed ultrasound frame showing acoustic reflector echoes. Green arrow highlights the echo from ① and the red arrow from ②. (c) A corresponding ultrasound A-line showing the acoustic reflector echoes.

ToF measurements **t**, local slowness map (hence SoS) can then be found by solving using an iterative computed tomography (CT) inverse problem [5]:

$$\hat{\mathbf{s}} = \arg\min_{\mathbf{s}} ||\mathbf{Ls} - \mathbf{t}||_1 + ||\mathbf{Ds}||_1 \qquad (1)$$

where **D** is a multi-angle anisotropically-weighted total variation (MA-AWTV) operator, which computes direction derivatives, and is the regularization weighting.

2.3. Acoustic properties of reflected echoes

Typically, a high acoustic impedance, smooth surface material is used as a reflector, for a high energy echo while keeping the wave-front in the imaging plane. As the reflector, we herein used a 5 mm thick, 100 mm wide Plexiglas, the acoustic properties of which (SoS=2670 m/s, density=1200 kg/m3) show good contrast with soft tissue (SoS=1540 m/s, density=1000 kg/m3). We designed an air gap beneath the reflector, as in [5], in order to have a chararacteristic secondary reflection (cf. Fig. 1a ②) with phase reversal, as in [5].

Assuming perfect reflections, preliminary methods [11] used normalized cross-correlation (NCC) with the transmitted wave. However, this feature (f_{NCC}) is unreliable given other reflections in the medium, e.g., skin, muscle, and fat layers. Given the fact that the first arrival wavefront should be of high amplitude, another intuitive feature is the location of maximum amplitude (f_{amp}) and/or gradient (f_{grad}). Phase symmetry (PS) feature (f_{PS}) was shown to be simple yet successful in delineating bone surfaces [12], and hence herein hypothesized to potentially be effective in detecting reflector echos as well. These above echo features, however, do not provide information regarding the temporal distribution of echo amplitude. In particular, reflector echoes are of high amplitude and are broader compared to other strong reflections from the tissue layers, often prepended with a low echogenic front. Therefore, similarly to the vessel and silicone pouch detector in [13], we herein also consider an edge filter of the form [-1,-1,...,-1, 1, 1,...,1] on the envelope data. We design the filter given the wave packet length w_l as $\sum_{n=1}^{w_l} x[t-n] - \sum_{n=1}^{w_l} x[t+n]$ to add values on the echo and to substract the cumulative sum prior to it (to find the first / rising
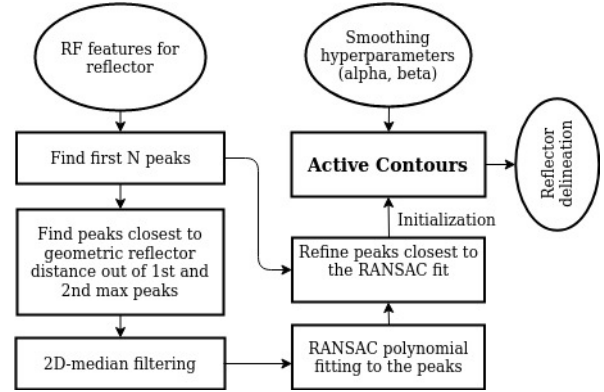
Fig. 2. Algorithmic flowchart of the proposed method.

peak of common reverberating echo trains), in practice by applying a filter kernel of length $2w_l$. Note that this feature (f_{filter}) brings out different echo characteristics compared to those earlier above based on echo shape that are highly influenced by dispersion and diffraction effects.

Since separate detections in individual A-lines can be error-prone, the prior that neighbouring Rx elements should have a similar ToF can be leveraged, such as using *active contours* for an energy minimization of a smooth contour (cf. across Rx A-lines in Fig. 1b) pulled towards desired echo features [10]. Active contours were used with a combination of amplitude and gradient features in [9]. However, active contour methods are highly sensitive to initialization and local minima, and can be affected by outliers. To address this concern, we herein propose to utilize optimal features for this problem, and then to cull best candidate locations using an outlier removal approach before applying an active contours approach (cf. Fig. 2).

2.4. Reflector delineation algorithm

In the first stage, for all Tx-Rx echo traces, we find the first n number of peaks of the corresponding feature values and select the 1st and 2nd peak positions, the majority of which belong to echoes from front (Fig. 1a ①) or back (Fig. 1a ②) reflector surface. We order the peaks based on their proximity to the transducer. In the next step, the selected location indices are first median filtered and then fitted using RANSAC [14] to a polynomial of the form $f(x) = a_n x^3 + \ldots + a_2 x^2 + a_1 x$, which represents an approximate reflector profile. This process ignores precise reflector delineation, nevertheless helps effectively remove outliers. Subsequently, precise timing locations are recovered by picking the points closest to the fitted polynomial from the initial n precise peaks. Note that these locations are likely not to be continuous (smooth) across Rx elements and still contain some outliers (e.g., at locations where the actual reflector echo was not in the first n peaks). We thus utilize a final active contour stage to find a smooth temporal curve for reflection delineation.

3. RESULTS AND DISCUSSION

We compare different features for reflector delineation, using only RANSAC, active contours initialized with features maxima locations (AC_{max}), and active contours initialized with RANSAC output (AC_{RANSAC}). To evaluate our proposed framework, we annotated the reflector locations in 128 multi-static Tx frames of a breast mimicking phantom, and report mean square error (RMSE) of different approaches to such gold standard. Knowing the expected reflector depth (i.e. it is not closer or farther than a certain depth) we used echo traces cropped between time samples 1500 and 2900 (corresponding to 37.5 us to 72.5 us). NCC is computed with a reference kernel selected from TX=63 & Rx=65 RF A-line leading to a length w_l of 26. We did not use Tx=Rx=64 or similar in order to avoid reverberations inherent to perfectly normal reflections. We used the following hyper-parameters optimized empirically. For f_{grad} feature, we use a derivative of Gaussian kernel with $= 2$. For f_{PS}, the number of scales set to 1, with a scale size of 26 and orientation angle of $90°$. Feature f_{amp} is obtained from the envelope of RF data, and involves no hyper-parameter. Since f_{amp} and f_{grad} features are known not be successful individually [7], we have combined them as in [9]. Their weighting factor for such combined $f_{grad}+f_{amp}$ is found via a grid search. For candidate retention, n is set to 4, with the candidates for one frame seen in Fig. 3(left:a). It is observed that these peaks contain not only the front reflector surface but also the back reflection (indeed most highest peaks are from there) as well other soft tissue reflections. After RANSAC with 128 iterations and a threshold of 450 ns outlier detection, the cubic fit seen in Fig. 3(left:b) is obtained. Active contours use a search range of 11 time samples and run until convergence, i.e. the sum of absolute difference (SAD) between two iterations is unchanged. Active contours elastic and curvature constants were identified with a grid search over, respectively, the ranges [0.01, 1] and [0.1, 10] with a step size 0.1.

For all 128x128 Tx-Rx pairs, the manually annotated ToF values as well as the AC_{RANSAC} results using different compared features are provided in Fig. 3(right:a). For each method, absolute differences from annotated results are shown in Fig. 3(right:b). The RMSE of AC_{RANSAC}, AC_{max}, and RANSAC alone are tabulated in Tab. 1 for different features.

It is observed that our proposed feature f_{filter} performs superiorly, regardless of the delineation pipeline. Across the three delineation algorithms, when using suboptimal features such as f_{PS} or $f_{amp}+f_{grad}$ then RANSAC alone can even perform slightly better than

Table 1. Root mean square error (RMSE) [ns] of three different delineation approaches using four different echo features as ToF candidate input. Right-most column tabulates the errors using only the Tx-Rx pairs within elements $f15,..,30g$, i.e. from a homogeneous tissue region (with minimal wavefront distortions). Total algorithmic runtimes for all Tx-Rx pairs are also reported.

Features	RANSAC	AC_{max}	AC_{RANSAC}	$AC_{RANSAC}^{homogen:}$
f_{PS} [15]	57.4	124.5	51.6	37.5
$f_{grad}+f_{amp}$ [9]	51.6	261.1	49.9	29.6
f_{NCC} [11]	39.2	35.8	35.6	24.1
f_{filter}	**29.0**	**26.1**	**26.1**	22.2
Time (s)	12	923	567	

AC based approaches. However, with f_{NCC} and f_{filter}, active contours is seen to be clearly superior over RANSAC alone. Iterative steps of active contours were implemented using dyanmic programming. For RANSAC and active contours, MATLAB (R2017a) implementations were used. All experiments were conducted with an Intel i7-2600K CPU @ 3.40 GHz and 16 GB RAM. Execution times for all 128 frames are reported in Tab. 1. Although the final delineation quality between two AC methods is not different with f_{filter} feature, AC_{RANSAC} with points pre-processed with RANSAC is seen to run almost twice faster compared to AC_{max} due to a better initialization and reduction in outliers. Speed of sound reconstructions with manually labelled as well as the SoS error maps of automatically delineated reflector profiles using AC_{RANSAC} are shown in Fig. 3(right:c). SoS RMSE with features f_{PS}, $f_{grad}+f_{amp}$, f_{NCC}, and f_{filter} are respectively 10.3, 7.9, 5.9, and 5.8 m/s.

In Fig. 3(right:b), one can see # shaped error bands for features f_{NCC}, $f_{grad}+f_{amp}$, and f_{PS}. These correspond to Rx and Tx combinations for diffracted reflector echoes passing around the edges of the inclusion. Given the diffractions and refractions around this inclusion boundary, the wavefronts are highly distorted. These are seen to produce errors while using several features, although our proposed f_{filter} is observed to be most robust to such wavefront distortions. This is also what mainly leads to the superior performance of the latter. Indeed, in the homogeneous phantom regions, e.g., for all Tx-Rx pairs within elements $f15,..,30g$, using most features (except f_{PS}) are seen to perform similarly; cf. the right-most column of Table. 1.

4. CONCLUSIONS

We have herein comparatively studied reflector delineation methods and shown that a custom edge filter crafted to reflector echo profile outperforms echo features proposed in the literature for this or similar purposes. Additionally, we have shown active contours to benefit from initialization and outlier removal via polynomial fitting with RANSAC. Resulting SoS maps are shown to have RMSE less than 10.3 m/s with respect to those reconstructed from manual echo delineations.

5. COMPLIANCE WITH ETHICAL STANDARDS

This is a tissue-mimicking phantom study for which no ethical approval was required.